Petroleum Science 21 (2024) 3804–3814

Contents lists available at ScienceDirect

Petroleum Science

journal homepage: www.keaipublishing.com/en/journals/petroleum-science

Original Paper

The generation mechanism of deep natural gas in Tabei uplift, Tarim Basin, Northwest China: Insights from instantaneous and accumulative effects

Xin Liu [a, b], Jin-Qiang Tian [a, b, *], Fang Hao [a, b, **], Ze Zhang [a, b, c], Xian-Zhang Yang [d], Yong-Quan Chen [d], Ke Zhang [d], Xiao-Xue Wang [d], Fu-Yun Cong [a, b]

[a] School of Geosciences, China University of Petroleum (East China), Qingdao, 266580, Shandong, China
[b] State Key Laboratory of Deep Oil and Gas, China University of Petroleum (East China), Qingdao, 266580, Shandong, China
[c] No.4 Gas Production Plant, PetroChina Changqing Oilfield Company, Xi'an, 710200, Shaanxi, China
[d] Research Institute of Petroleum Exploration and Development, PetroChina Tarim Oilfield Company, Korla, 841000, Xinjiang, China

ARTICLE INFO

Article history:
Received 13 December 2023
Received in revised form
1 July 2024
Accepted 13 August 2024
Available online 14 August 2024

Edited by Jie Hao

Keywords:
Instantaneous gas generation
Carbon isotope
Hydrocarbon accumulation
Spatial variation
Tarim basin

ABSTRACT

The natural gas heavy carbon isotope and high dryness coefficients genesis in Tabei uplift, Tarim Basin has been highly controversial. To investigate the generation mechanisms of natural gas in the Tabei Uplift. Natural gas chemical composition, carbon isotopes were used to analyze the genesis of natural gas, source rock maturity, and basin modeling were conducted to reconstruct the natural gas generation process, and the influences of instantaneous and cumulative effects on natural gas properties was discussed. The results show that the dryness coefficients of natural gas range from 0.62 to 0.99 (average: 0.92), the methane contents range from 30.42% to 96.4% (average: 85.10%), ethane contents from 0.43% to 15.58% (average: 3.39%), propane contents from 0.11% to 11.43% (average: 1.78%), and the methane carbon isotopes range from −47.30‰ to −33.80‰ (average: −36.96‰), ethane carbon isotopes range from −39.60‰ to −33.20‰ (average: −35.57‰), propane carbon isotopes range from −36.90‰ to −28.50‰ (average: −35.49‰). Compared with the actual regional thermal evolution of the source rock (R_o% range from 1.4%–1.7%), the natural gas exhibits excessively high dryness coefficients and heavy methane carbon isotope characteristics. The natural gas is primary cracking gas and sourced from marine type II kerogen. The dryness coefficient, methane carbon isotopes, and source rock maturity gradually increases from the west to the east. Instantaneous effects and leakage led to the dry gas and relative heavy methane carbon isotopes generated at a low maturity level. The current natural gas in the Ordovician reservoirs was all generated during the Himalayan orogeny. Long period pause of the gas generation between the two hydrocarbon generation phases is the main cause for the instantaneous effects.

1. Introduction

The natural gas resources in China are abundant and come from a diverse range of sources (Dai et al., 2009; Zhu et al., 2009, 2014). In recent years, the Tarim Basin has made significant breakthrough in deep and ultra-deep hydrocarbon exploration, and is one of the most petroliferous basins in China, with natural gas reserves exceeding 1.1 × 10^{12} m^3 (Zhu et al., 2014; Cong et al., 2021; Li et al., 2022). Currently, the Tabei uplift is an important natural gas producing area in the Tarim Basin, and the natural gas reserves exceed 4.69 × 10^{11} m^3 (Yang et al., 2016; Chen et al., 2020b). The Lunnan area is the richest natural gas-producing area in the Tabei uplift. In the Lunnan area, a large amount of oil and gas has been found in reservoirs within different formations, and the Ordovician reservoir is the most important hydrocarbon-bearing interval (Zhou and Zhang, 2000; Wang and Zhang, 2010; Wu et al., 2013; Chen et al.,

* Corresponding author. School of Geosciences, China University of Petroleum (East China), Qingdao, 266580, Shandong, China.
** Corresponding author. School of Geosciences, China University of Petroleum (East China), Qingdao, 266580, Shandong, China.
E-mail addresses: tianjq@upc.edu.cn (J.-Q. Tian), haofang@cug.edu.cn (F. Hao).

https://doi.org/10.1016/j.petsci.2024.08.002

2020a; Zhang et al., 2022).

Natural gas generation in sedimentary basins occurs in two main ways: thermal cracking of organic matter and microbial activity. The properties of microbial gases are not related to the type of organic matter, and is primarily influenced by temperature and the pathway of methanogenic by methanogens, and the alkane gases produced under the influence of microbial activity are generally lighter in carbon isotopes than thermogenic gas in this case (Schoell, 1980). On the other hand, thermogenic gas includes three main ways: kerogen cracking gas, oil-cracking gas, and wet gas cracking gas (Prinzhofer and Huc, 1995; Lorant et al., 1998). And due to the different organic precursors, the chemical composition and stable isotopes of thermogenic gas generated were vary significantly.

In recent years, several investigators have examined different aspects of gas properties and geochemical characteristics of the Ordovician natural gas in the Lunnan area. Most of the analysis focused on natural gas genesis, migration and charging processes, gas sources, and later chemical modification (Wu et al., 2013; Liu et al., 2017; Zhu et al., 2019, 2020; Chen et al., 2020a; Wang et al., 2021; Zhang et al., 2022). Previous research suggests that the Ordovician natural gas in the Lunnan area is dominated by kerogen cracking gas (Wang and Zhang, 2010; Liu et al., 2017; Yu et al., 2022). The dryness coefficients exhibit characteristics of high values in the east (with an average value of 0.98) and low values in the west (the average value of dryness coefficient is 0.74). The methane carbon isotopes show characteristics of heavy values in the east (with an average value of −34.81‰) and light values in the west (with an average value of −42.06‰) (Zhu et al., 2019; Chen et al., 2020a; Zhang et al., 2022). Furthermore, to reach such characteristics of dryness coefficients and methane carbon isotopes, as scholars claimed, the source rock maturity should be exceeding 2% in the Lunnan area (Peng and Jia, 2021). But the actual source rock maturity is only 1.4%–1.7%, corresponding to the stage of thermal cracking to generate condensate gas. Although obvious spatial variation in gas chemical properties has been observed in the field, consensus on the potential causes has not been reached. Previous research suggests such phenomenon may be related to the long-distance lateral migration causing the isotopic fractionation or highly efficient hydrocarbon expulsion efficiency (Wu et al., 2013; Zhu et al., 2020). And even some investigators proposed the existence of deeper Sinian source rock with higher maturity in the Tabei uplift. But with the advances in exploration and the increase in data volume, the simple lateral migration model is inadequate in explaining the complex patterns of natural gas properties and their spatial changes, and highly efficient hydrocarbon expulsion efficiency can't lead to the generation of dry gas and heavy methane carbon isotopes at relatively low source rock maturity stages (Chen et al., 2020a; Zhu et al., 2020). Such seemingly decoupling between source rock thermal maturity and gas properties (wetness coefficient, isotopic ratios) of natural gas in the Lunnan area remains highly controversial.

In this study, using the natural gas components and carbon isotope data, and integrating gas-generation simulation, we aim to analyze the genesis of natural gas, and unravel the geologic causes of the spatial variation in geochemical properties of natural gas in the Tabei uplift.

2. Geological setting

The Tarim Basin is located in the northwestern China, it is the largest petroleum-bearing basin in China with an area of 56×10^4 km^2 (Fig. 1) (Jiang et al., 2017; Yao et al., 2018; Yang et al., 2020; Cong et al., 2022). The Tarim Basin can be categorized into the Northern depression belt, the Southeastern depression belt, the Kuqa depression belt, the Southwestern depression belt, the Central uplift belt, the Tabei uplift, and the Southeastern uplift belt basing on its tectonic zoning. The Northern depression belt comprises the Manjiaer depression, the Awati depression, and the Shuntuoguole low uplift (Jia and Wei, 2002; Yu et al., 2011; Jiang et al., 2015; Cong et al., 2021). The study area is located in the Lunnan area, the eastern part of the Tabei Uplift (Wang and Zhang, 2010; Yang et al., 2016; Zhang et al., 2022).

The Lunnan area develops "X" conjugate strike-slip faults, with planes striking in the NEE and NNW directions and intersecting at a diamond-shaped tangent (Fig. 1(c)). The large fracture zones are mainly including the Luntai fault, the Lunnan fault, the Sangtamu fault and the Lungudong fault, all of which penetrate through multiple stratigraphic intervals (Wang and Zhang, 2010; Deng et al., 2019; Chen et al., 2020a Wu et al., 2021).

The Lunnan area underwent six major tectonic evolution stages, and underwent sedimentary filling from the Quaternary to the Ediacaran strata (Chen et al., 2020a). Due to the tectonic activities, the strata suffered uplift and erosion, and ultimately resulted in the lack of the Permian, Ediacaran and Devonian strata (Fig. 2). During the Caledonian orogeny, the Cambrian and Ordovician strata were deposited, and the Cambrian to Middle-Lower Ordovician are dominated by carbonate sediments, whereas the Upper Ordovician intervals comprise thick dark gray mudstone with thin limestone interlayers (Jiang et al., 2016). Recent studies have concluded that Cambrian Yuertusi Formation is the most dominant source rock (Zhu et al., 2018), with the Ordovician carbonate strata developed as one of the major reservoir intervals. During the Hercynian orogeny, the Carboniferous strata was deposited, and the lithofacies consists mainly of limestone and clastic rock. During the Yindo-China, Yanshan, and Himalayan orogeny, the Triassic, Jurassic and Cretaceous, Paleogene to Quaternary strata were deposited, respectively, with mudstone and sandstone being the main lithofacies. In the Lunnan area, the Cambrian-Ordovician stratigraphic sequences from young to old include the Lianglitage Formation (O_3l), Sangtamu Formation (O_3s), Tumuxiuke Formation (O_3t), Yijianfang Formation (O_2yj), Yingshan Formation ($O_{1\text{-}2}y$), Penglaiba Formation (O_1p), Qiulitage Formation (ϵ_3q), Awatage Formation (ϵ_2a), Shayilike Formation (ϵ_2s), Wusonggeer Formation (ϵ_1w), Xiaoerbulake Formation (ϵ_1x), Yuertusi Formation (ϵ_1y) (Fig. 1(d)).

3. Samples and analytic methods

3.1. Samples

A total of 49 samples were used in this study, of which 10 natural gas sample data (from Sinopec Northwest China Petroleum Bureau) were obtained by citing previous literature (Table 1), and the rest of the well samples were wellhead gases collected by travelling to the Lunnan Oil and Gas Production Management Area, Tarim Oilfield, Petrochina using stainless steel cylinders. The sampling procedure was to open the valves on both sides of the cylinders and each cylinder was flushed for 3–5 min to remove any air contamination., then close the valve on one side and continue to fill the gas for 1–2 min and then close the valve. It is important to note that the pressure inside each cylinder was maintained at a high level of 1–4 MPa.

3.2. Data and methods

All samples preparation and measurements were finished in the State Key Laboratory of Deep Oil and Gas in China University of Petroleum (East China), and Geochemistry Laboratory in China University of Petroleum (Beijing). Natural gas chemical component analysis was carried out on Agilent 6890N chromatograph at the

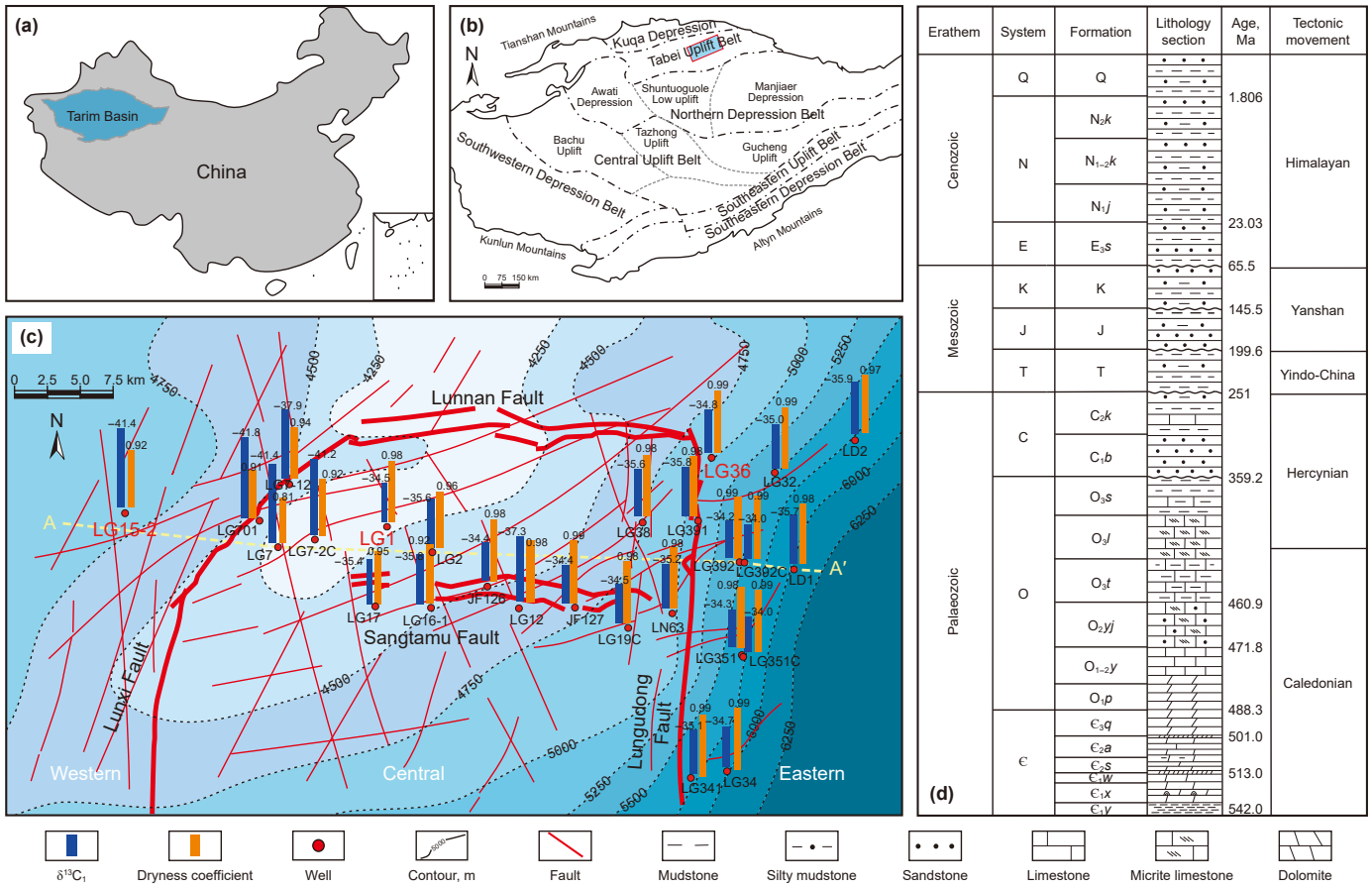

Fig. 1. **(a)** Location of the Tarim Basin, China; **(b)** Location of the study area in the northern Tarim Basin; **(c)** Structural map of the Ordovician strata showing the fault distribution, dryness coefficient and methane carbon isotope spatial variation in the Lunnan area; **(d)** Comprehensive stratigraphic column for the Tabei Uplift, Tarim Basin (modified after Zhu et al., 2020). Q = Quaternary; N=Neogene; E = Paleogene; K=Cretaceous; J = Jurassic; T = Triassic; C=Carboniferous; O=Ordovician; Є = Cambrian.

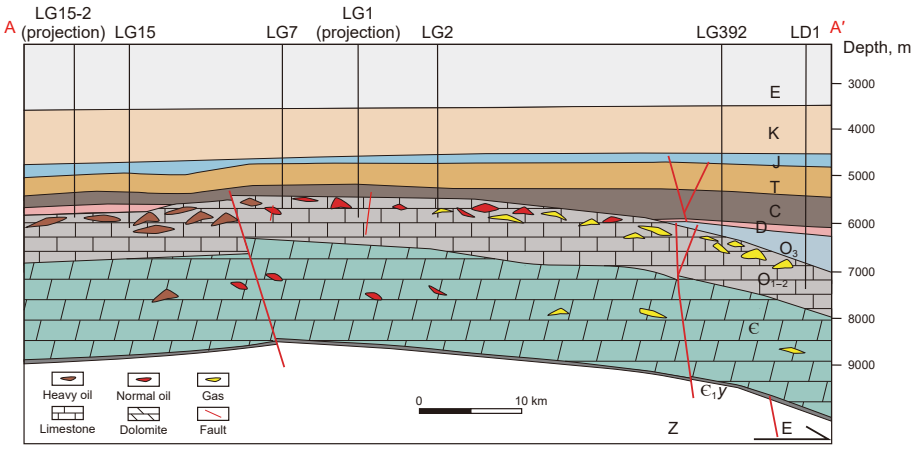

Fig. 2. Cross section showing the stratigraphic framework and fault distribution in the Lunnan area (line mark A-A′ in Fig. 1).

China University of Petroleum (Beijing). The column temperature was maintained at a constant temperature of 60 °C, the injector temperature was maintained at 100 °C, the carrier gas was helium at a flow rate of 1 mL/min, and the detector temperature was 200 °C.

Natural gas carbon isotope components analyze was carried out on Thermo Fisher MAT 253plus (GC-IRMS) in Key Laboratory of Deep Oil and Gas in China University of Petroleum (East China). The chromatographic column was a 30 m × 320 mm PLOT Q, the flow rate of carrier gas was 1.8 mL/min, the oven temperature was 80 °C, and the heating procedure was to keep the initial temperature at 25 °C for 5 min, and then gradually increase the temperature to 80 °C at 2 °C/min. The carbon reactor temperature was 1000 °C. The reported stable carbon isotope values are δ-labelled values in millimeters (‰) relative to the Vienna Pewee Dolomite Standard (VPDB), with a reproducibility of ±0.3‰ for δ13C measurements. In

Table 1
The chemical and carbon isotopic compositions of natural gas from the marine carbonate gas reservoirs in the Tabei uplift (part datas are from Gao et al. (2005)).

Areas	Wells	Strata	Chemical composition, %							Carbon isotope composition, %					Dryness coefficients
			CH_4	C_2H_6	C_3H_8	iC_4H_{10}	nC_4H_{10}	iC_5H_{12}	nC_5H_{12}	$\delta^{13}C_1$	$\delta^{13}C_2$	$\delta^{13}C_3$	$\delta^{13}iC_4$	$\delta^{13}nC_4$	
Eastern area	LD1	O	88.90	1.65	0.51					−35.70	−37.10	−33.40	−30.40	−29.90	0.98
	LD2	O	93.40	2.39	0.42					−35.90	−36.60	−32.30	−29.40	−30.10	0.97
	LG32	O	91.50	1.02	0.21	0.04	0.10	0.04		−35.00	−37.50	−36.90	−32.10	−30.80	0.98
	LG34	O	94.50	0.95	0.16	0.03	0.06	0.02	0.03	−34.70	−33.90	−30.60	−29.00	−30.20	0.99
	LG341	O	93.90	0.85	0.18	0.05	0.09	0.05		−35.10	−33.40	−29.40	−30.70	−30.50	0.99
	LG351	O	64.70	0.56	0.15	0.03	0.09	0.08	0.13	−34.30	−36.90				0.98
	LG351C	O	96.40	0.93	0.24	0.04	0.09	0.02		−34.00	−35.10	−33.50	−31.00	−31.80	0.99
	LG36	O	91.70	0.63	0.11	0.01	0.03	0.01		−34.80	−37.50	−32.90		−36.80	0.99
	LG391	O	93.80	1.12	0.30	0.05	0.10	0.03	0.04	−35.80	−38.10	−34.70		−33.70	0.98
	LG392	O	42.20	0.43	0.13	0.02	0.06	0.03		−34.20	−34.50				0.98
	LG392C	O	83.10	0.63	0.11	0.02	0.04	0.01		−34.00	−33.30	−30.90	−29.50	−30.40	0.99
	LN63	O	94.18	1.18	0.38	0.06	0.16	0.05	0.07	−35.20	−38.50	−34.80		−31.80	0.98
	LN631	O	94.40	0.95	0.32	0.29				−33.80	−33.80	−31.20	−30.50		0.98
Central area	JF126	O	94.26	1.06	0.59	0.43				−34.40	−33.70	−30.50			0.98
	JF127	O	95.34	0.51	0.24	0.16				−34.40	−33.20	−30.80	−28.30		0.99
	LG101	O	92.51	2.46	0.84	0.21	0.36	0.11	0.11	−34.40	−33.70	−30.00			0.96
	LG102	O	94.54	1.39	0.39	0.09	0.17	0.05		−34.20	−34.00	−30.60	−28.30	−29.10	0.98
	LG12	O	95.40	1.16	0.36	0.23				−37.30	−33.20	−34.00			0.98
	LG16-2	O	92.50	2.00	0.82	0.18	0.32	0.10	0.11	−34.20	−34.80	−31.60	−30.40	−29.40	0.96
	LG16C	O	90.97	2.13	0.84	0.21	0.33	0.11	0.12	−35.50	−35.30	−32.10	−31.70	−30.90	0.96
	LG17	O	91.10	2.65	1.06	0.26	0.41	0.14	0.13	−35.40	−33.40	−31.50			0.95
	LG18	O	95.10	1.18	0.29	0.19				−34.80	−33.90	−32.50			0.98
	LG19C	O	76.91	0.90	0.21	0.04	0.07	0.02	0.02	−34.50	−34.10	−30.60	−27.30	−28.50	0.98
	LG38	O	94.30	1.21	0.29	0.10		0.04		−35.60	−38.30	−35.10	−27.50	−34.10	0.98
	LN634	O	94.85	1.31	0.47	0.38				−34.60	−34.30	−31.60	−30.70		0.98
	LG16-1	O	87.8	4.48	2.64	0.76		0.2		−35.80	−35.10	−32.70	−31.40		0.92
	LG1	O	91.25	1.54	0.25	0.08	0.13	0.04		−34.50	−33.30	−28.60		−29.50	0.98
	LG100-11	O	91.50	2.11	0.81	0.37	0.21			−35.50	−34.10	−31.40	−30.60		0.96
	LG100-6	O	95.08	1.99	0.37	0.10	0.16	0.06	0.07	−34.90	−34.80	−32.20	−30.20	−30.60	0.97
	LG111	O	94.70	1.32	0.38	0.09	0.15	0.04	0.05	−34.00	−33.40	−30.60	−28.20	−28.60	0.98
	LG2	O	90.20	2.37	0.92	0.11	0.24	0.06	0.09	−35.60	−38.60	−35.40		−32.20	0.96
	LG21	O	93.30	1.33	0.41	0.10	0.19	0.07	0.08	−35.90	−33.90	−30.90	−28.90	−29.50	0.98
	LG4	O	92.42	1.72	0.55	0.00	0.00	0.00	0.00	−37.94	−34.30	−31.84	−31.31	−31.27	0.98
	LG7-12	O	91.70	3.95	1.39	0.24	0.36	0.07	0.07	−37.90	−34.60	−32.70	−32.50	−32.40	0.94
	LN39-1	O	94.20	1.60	0.59	0.39				−33.90	−34.50	−31.40	−30.20		0.97
	LG701	O	77.5	5.06	2.54	0.81		0.24		−41.80	−38.70	−34.60	−30.90		0.91
	LG7	O	72.1	8.56	6.65	2.71		0.82		−41.40	−39.60	−35.60			0.81
	LG7-2C	O	80.8	4.02	2.49	1.23		0.61		−41.20	−35.50	−34.70	−33.20		0.92
	AT24X	O								−41.20	−36.60	−33.00	−32.30	−31.50	0.80
	S47	$O_{1-2}y$	86.35	6.31	3.11					−40.70	−35.20	−33.30			0.88
	TK228	O_{1-2}	78.63	7.27	4.84					−40.40	−39.20	−35.30			0.83
Western area	LG15-2	O	81.86	4.95	1.29	0.25	0.39	0.08	0.08	−41.40	−39.60	−36.00	−33.60		0.92
	TP35CX-1	O								−46.40	−37.60	−33.60	−32.80	−31.70	0.73
	TP39	O	61.19	15.58	11.43	2.33	3.95	1.61	2.02	−39.30		−28.50	−29.20	−28.20	0.62
	TP42	O	65.02	14.56	7.23	1.08	1.22	0.33	0.24	−47.30	−35.00	−31.40	−30.90	−29.20	0.73
	YQX1	O	30.42	6.17	4.07	0.67	1.3	0.31	0.29	−41.50	−36.70	−32.90	−32.80	−31.00	0.70
	S112	O_3l	71.83	12	7.13					−43.00	−34.60	−32.20			0.74
	S106	O1-2y	72.99	9.29	7.08					−40.10	−38.40	−34.20			0.76
	TK720	O1-2y	68.41	11.7	7.84					−37.50	−35.80	−33.10			0.72

our laboratory, the methane, ethane, and propane standards are $\delta^{13}C_1 = -43.61 \pm 0.09‰$, $\delta^{13}C_2 = -40.24 \pm 0.10‰$ and $\delta^{13}C_3 = -33.79 \pm 0.09‰$. The values can reach the VPDB international carbon isotope standard (Dai et al., 2012).

The 1D Source rock maturity and burial history simulation of LG15-2, LG1, LG36 wells in the Tabei oil fields were performed using Petromod software. Parameters such as stratigraphic layers, depositional ages, fault properties, facies (including lithology, petroleum system elements and source rock properties) and boundary conditions (including erosion thickness, palaeo-water depth, palaeo-surface temperature and heat flow) were input. Stratigraphic layers, lithology, and erosion thickness were taken from the well completion reports provided by PetroChina Tarim Oilfield Company. The heat flow refers to Li et al. (2010) results, and combined with the measured Ro% to make appropriate adjustments. Petroleum system elements include the lower Cambrian Yuertusi source rock interval, Ordovician reservoir and upper strata intervals. Since the target wells were not drilled to encounter the hydrocarbon source rocks of the Lower Cambrian Yuertusi Formation (~9000–10000 m), the source rock attributes of the LT1 well drilled to encounter the Yuertusi Formation in the Lunan area (with an average TOC content of 9.5%) were used as the reference values for inputting into the model when modelling the hydrocarbon generation history. The hydrocarbon generation kinetics refers to models proposed by Dieckmann et al. (2000).

4. Results

4.1. Chemical composition of the natural gas

The Ordovician natural gas chemical characteristics from the west to the east display vast variation in the Lunnan area. It may have been influenced by a variety of factors such as gas source, maturity, and reservoir generation process (Schoell, 1988; Jenden

et al., 1993; Prinzhofer and Huc, 1995; Whiticar, 1999). In the Lunnan area, the methane contents range from 30.42% to 96.4% (average: 85.10%), ethane contents from 0.43% to 15.58% (average: 3.39%), propane contents from 0.11% to 11.43% (average: 1.78%), and the dryness coefficients from 0.62 to 0.99 (average: 0.92) (Table 1). In the western area, natural gas is dominated by wet gas, and the methane contents range from 30.42% to 81.86% (average: 64.53%), ethane contents from 4.95% to 15.58% (average: 10.61%), propane contents from 1.29% to 11.43% (average: 6.58%), and the dryness coefficients from 0.62 to 0.92 (average: 0.74) (Table 1). In the central area, natural gas consists of wet and dry gas, and the methane contents range from 72.10% to 95.40% (average: 89.83%), ethane contents from 0.51% to 8.56% (average: 2.65%), propane contents from 0.21% to 6.65% (average: 1.27%), and the dryness coefficients from 0.80 to 0.99 (average: 0.94). In the eastern area, natural gas is dominated by dry gas, and the methane contents range from 42.20% to 96.40% (average: 86.36%), ethane contents from 0.43% to 2.39% (average: 1.02%), propane contents from 0.11% to 0.51% (average: 0.25%), and the dryness coefficients from 0.97 to 0.99 (average: 0.98) (Table 1).

4.2. Carbon isotope of natural gas

In the Lunnan area, methane carbon isotopes are distributed in the range from −47.30‰ to −33.80‰ (average: −36.96‰), ethane carbon isotopes are distributed in the range from −39.60‰ to −33.20‰ (average: −35.57‰), propane carbon isotopes are distributed in the range from −36.90‰ to −28.50‰ (average: −35.49‰). Significant spatial variation in carbon isotopes of gas can be observed from the west to the east (Fig. 3).

In the western area, methane carbon isotopes are distributed in the range from −47.30‰ to −37.50‰ (average: −42.06‰), ethane carbon isotopes are distributed in the range from −39.60‰ to −34.60‰ (average: −36.81‰), propane carbon isotopes are distributed in the range from −36.00‰ to −28.50‰ (average: −32.74‰). The natural gas carbon isotopes show normal sequence ($\delta^{13}C_{methane}<\delta^{13}C_{ethane}<\delta^{13}C_{propane}<\delta^{13}C_{butane}$). In the central area, methane carbon isotopes are distributed in the range from −41.80‰ to −33.90‰ (average: −36.50‰), ethane carbon isotopes are distributed in the range from −39.60‰ to −33.20‰ (average: −35.12‰), propane carbon isotopes are distributed in the range from −35.60‰ to −28.60‰ (average: −32.33‰). The overall carbon isotopic composition of the alkanes follows the trend of normal sequence ($\delta^{13}C_{methane}<\delta^{13}C_{ethane}<\delta^{13}C_{propane}<\delta^{13}C_{butane}$), but partial reversal ($\delta^{13}C_{methane}>\delta^{13}C_{ethane}$) also exists in a few wells (Fig. 4). In the eastern area, methane carbon isotopes are

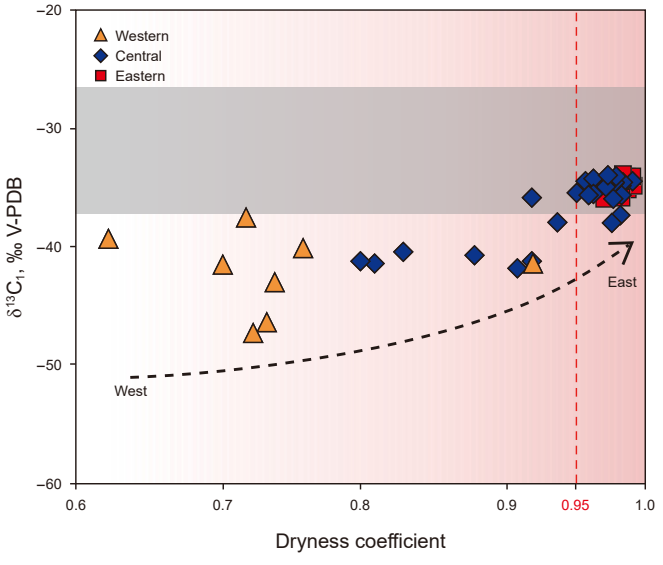

Fig. 3. The correlation diagram between $\delta^{13}C_1$ vs. Dryness coefficient in the Lunnan area.

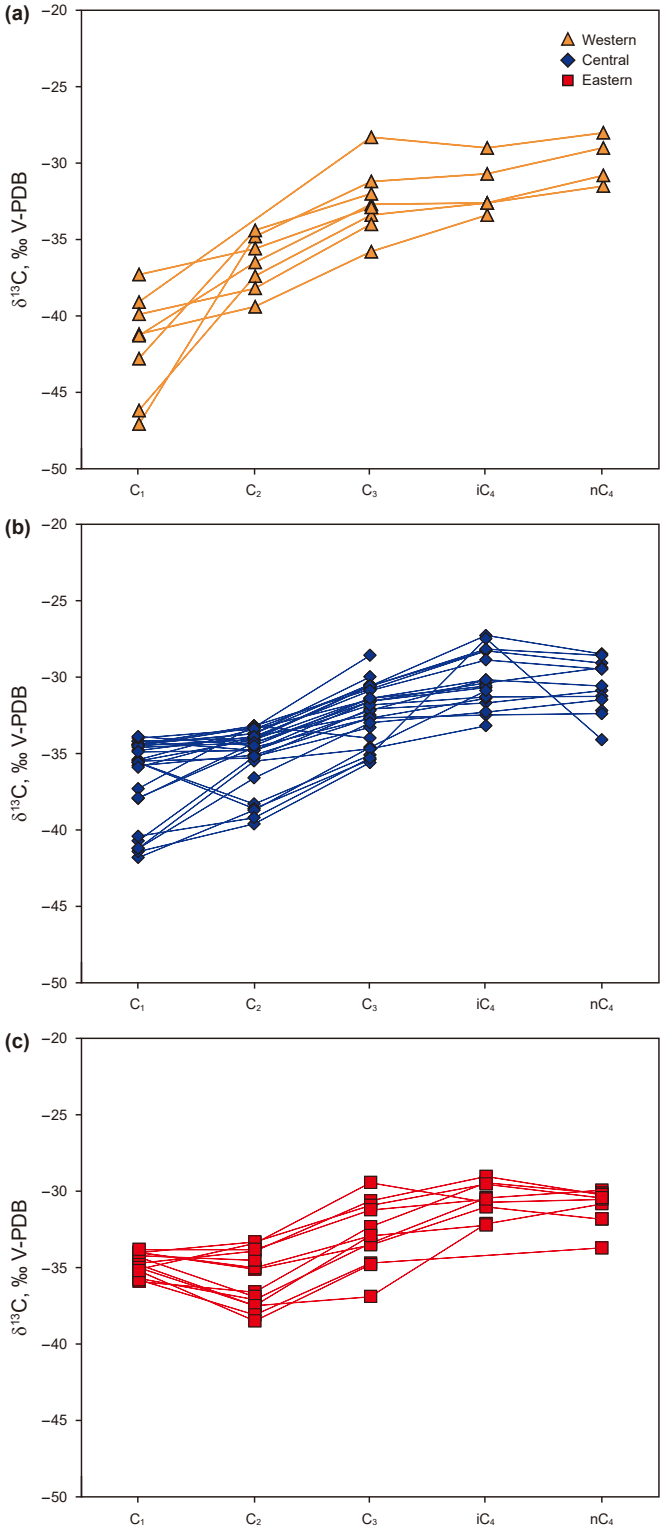

Fig. 4. Chung plot of 1/Cn vs. $\delta^{13}C$ values in the Lunnan area.

distributed in the range from −35.90‰ to −33.80‰ (average: −34.81‰), ethane carbon isotopes are distributed in the range from −38.50‰ to −33.30‰ (average: −35.86‰), propane carbon isotopes are distributed in the range from −36.90‰ to −29.40‰ (average: −32.78‰). There are significant differences in the carbon isotope relationships of methane and ethane between the east and west areas of the Lunnan area. Due to the higher source rock maturity in the eastern area, methane carbon isotopes are heavier in the east than the west (Fig. 4). In the western area, the methane carbon isotopes and ethane carbon isotopes show normal sequence ($\delta^{13}C_{methane}<\delta^{13}C_{ethane}$). However, compared to the western area, the methane carbon isotope values are significantly heavier in the central and eastern area, meanwhile, ethane carbon isotopes also show a very weak increasing trend, similar to the experimental simulations of Berner and Faber (1996), but the ethane carbon isotopes do not display such obvious spatial variation.

4.3. The variation of typical wells modeled source rock maturity and subsidence processes

The results of burial and thermal history modelling show large differences in subsidence and maturation processes of the in-situ source rock of the Yuertusi Formation in different areas of the Lunnan area. From the Caledonian to the late Hercynian orogeny (~542–251 Ma), the Yuertusi Formation strata continues to subside and the source rock maturity gradually increases. During the late Hercynian to the Yanshan orogeny (~251–65.5 Ma), the strata's burial depth shows minimal change, and thus no significant increase was manifested in the source rock maturity. During the Himalayan orogeny (<65.5 Ma), the strata experienced rapid burial within a relatively short period, leading to a rapid increase in the maturity of the source rock. From west to east, the burial depth gradually increases, resulting in source rock exhibiting higher maturity in the eastern area compared to that in the western area (Fig. 5).

Differences in the burial history at different periods and in areas result in significant variations in source rock maturity and hydrocarbon generation conditions. From the Caledonian to the early Hercynian orogeny (~542–359.2 Ma), the maturity of the in-situ source rock in LG15-2, LG1, and LG36 wells increased to 0.76%, 0.80%, and 0.90%, respectively, accompanied by continuous hydrocarbon generation (Fig. 5). During the late Hercynian orogeny (~299–251 Ma), the maturity of the in-situ source rock in LG15-2, LG1, and LG36 wells increased to 1.05%, 1.12%, and 1.20%, resulting in relatively abundant hydrocarbon generation. During the late Hercynian to the Yanshan orogeny (~251–65.5 Ma), there was no significant change in maturity of the in-situ source rock over an extended period, leading to a pause in hydrocarbon generation. During the Himalayan orogeny (<65.5 Ma), the burial depth and source rock maturity of LG15-2, LG1, and LG36 wells rapidly increased from 1.12% to 1.41%, 1.23%–1.51%, 1.36%–1.68% within a short period, respectively, and this period is the primary natural gas generation phase (Zhang et al., 2022; Zhao et al., 2022).

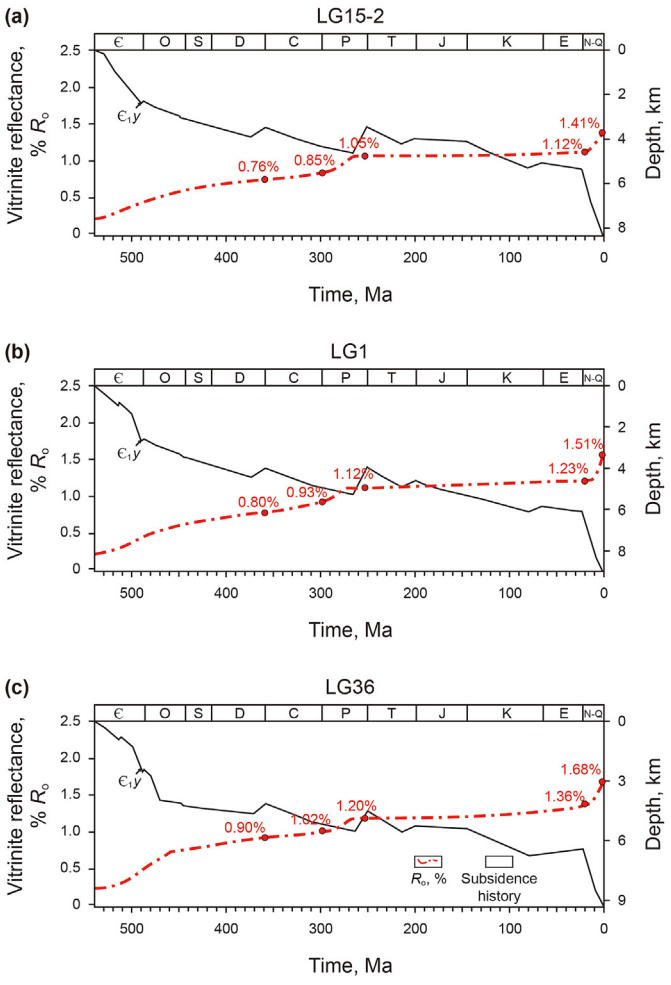

Fig. 5. Source rock maturity evolution and subsidence history simulations of the Yuertusi Formation in the Lunnan area (LG15-2: Western area, LG1: Central area, LG36: Eastern area).

5. Discussion

5.1. Genesis of natural gas

The stable chemical composition and hydrocarbon isotopic values of natural gas are crucial in identifying its genetic types (Whiticar, 1999; Liu et al., 2017). The Whiticar plot is useful in identifying the types of gas-producing kerogen by utilizing methane carbon isotopes and natural gas chemical compositions ($C_1/(C_2+C_3)$ vs $\delta^{13}C_1$) (Whiticar, 1999). As revealed in Fig. 6(a), all the natural gas in the Lunnan area can be classified into thermal cracking gas, with marine type II kerogen being the source. There are significant differences in natural gas maturity between the east and west areas of the Tabei uplift, with maturity increasing gradually from the west to the east. Identification of oil-cracking gas and kerogen cracking gas can be accomplished through diagrams such as $Ln(C_1/C_2)$ vs $Ln(C_2/C_3)$ and $Ln(C_2/C_3)$ vs $\delta^{13}C_2-\delta^{13}C_3$ (Prinzhofer and Huc, 1995). Fig. 6 (b) and (c) suggests that gas in the Lunnan area is dominated by kerogen cracking gas.

The carbon isotope composition of natural gas reflects the organic matter type and the degree of thermal evolution (Stahl, 1973; Stahl and Carey, 1975). When organic matter undergoes a simple thermal cracking reaction, the carbon isotopes of methane, ethane, and propane follow the normal sequence trend ($\delta^{13}C_{methane}<\delta^{13}C_{ethane}<\delta^{13}C_{propane}$) (Chung et al., 1988). It was found that most of the natural gas isotopes in the Lunan area are in the normal sequence, but some samples exist reversal. Natural gas in gas reservoirs may undergoes complex geological processes, such as heavy hydrocarbon gas cracking, mixing of multiple source gases, biodegradation, thermochemical sulfate reduction (TSR), gas diffusion/leakage, and gas invasion, etc. These conditions would significantly alter the chemical properties of natural gas, leading to isotope reversal (Chung et al., 1988; Waples, 2000; Cao et al., 2005; Fusetti et al., 2010; Huang and Li, 2017; Liu et al., 2017). The latest

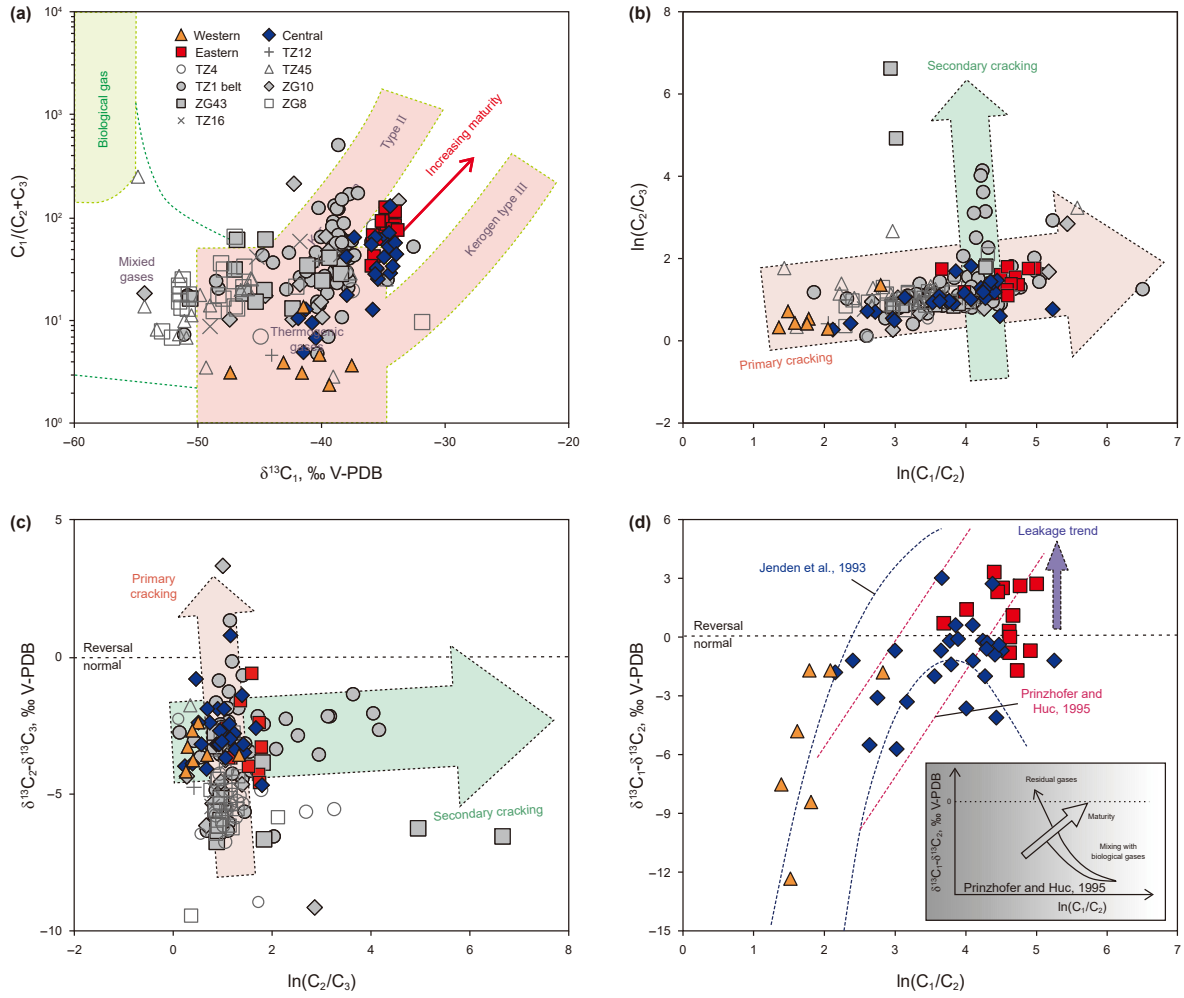

Fig. 6. The diagram of genesis of natural gas in the Lunnan area (modified after Prinzhofer and Huc, 1995; Whiticar, 1999).

studies have concluded that the natural gas in the Tarim Basin is mainly generated from Cambrian source rock, so the difference in its precursors type can be ruled out. The natural gas is mainly kerogen cracking gas as discussed previously. Significant biodegradation and TSR effects were also not found in previously reported natural gas geochemical characteristics. However, there is significant leakage of natural gas in the Lunnan area (Fig. 6(d)), which leads to the residual methane carbon isotopes becoming heavier, even partially heavier than the ethane carbon isotopes, which is the main reason for the isotopic reversal.

5.2. Natural gas generation process of source rock

The source rock maturity (R_o%) is a critical indicator for identifying whether oil or gas is generated (Harouna et al., 2017). Analyzing the regional burial history and its correlation with the spatial variation of source rock maturity of the Cambrian Yuertusi Formation in the Lunnan area is essential for exploring the generation process of natural gas.

In the eastern area, the higher maturity of the source rock and leakage results in generating natural gas with a higher dryness coefficient and heavier methane carbon isotopes compared to that in the western area, and even a few gas samples exhibit isotope reversal with carbon isotope of methane heavier than that of ethane (Fig. 4). Natural gas dryness coefficient shows the characteristics of higher in the east and decreasing towards the west, which may be related to the deeper burial depth and therefore higher maturity of the source rock in the east, and thus lead to relatively higher degree of gas maturity.

Noteworthy, the above-mentioned co-variation in burial history of in-situ source rock and gas properties implies a seemingly causal relationship between the thermal maturity and gas-generation processes of the in-situ buried source rock with the geochemical properties of natural gas. The source rock maturity in the east and west reaches the condition necessary for natural gas generation. However, it does not reach the condition for the large accumulation of dry gas (with a dryness coefficient of >0.95) (Dai et al., 2016). Therefore, the evolution of source rock thermal maturity can only explain the gradual increase in source rock maturity, natural gas dryness coefficient, and carbon isotopes from the west to the east in the Lunnan area, it still cannot explain the presence of a large amount of dry gas enriched in ^{13}C in the central and eastern areas. The reasons for the genesis of heavy methane carbon isotopes and dry gas in the eastern area are discussed below, by introducing the effects of instantaneous and accumulative gas generation processes.

5.3. The impacts of instantaneous and accumulative effects on natural gas properties

The properties of natural gas are influenced by various factors

such as source rock maturity, organic matter type, and natural gas generation process (Tang et al., 2000; Li et al., 2004; Tian et al., 2010; Liao et al., 2015; Li et al., 2019). In the Lunnan area, gas generation modelling results indicate that the source rock generated a lot of natural gas during the late Hercynian and Himalayan orogeny, and dryness coefficient of the generated gas in the eastern area is generally higher than that in other areas. However, this cannot explain why the Lunnan area has generated a large amount of dry gas with anomalously heavy methane carbon isotopes at a relatively low source rock maturity. Two distinct pathways for thermogenic gas generation were proposed based on pyrolysis experiments and numerical simulation, i.e., the accumulative gas generation process and the instantaneous gas generation process (Fig. S3) (Behar et al., 1995; Rooney et al., 1995; Tang et al., 2000). Both processes could exert significant impact on the properties of natural gas.

The accumulative gas process preserves both early and late gas generated by the source rock, while the instantaneous gas process only preserves late generated gas (Schoell, 1988; Schenk and Horsfield, 1993; Rooney et al., 1995; Cramer et al., 2001; Liao et al., 2015). Furthermore, there are significant differences in the natural gas carbon isotopes and dryness coefficients generated at different maturity levels for accumulative and instantaneous gas (Behar et al., 1995, 1997; Cramer et al., 2001; Chen et al., 2022a; Tian et al., 2023). By comparing the isotope and compositional results acquired from pyrolysis experiments and numerical simulation in previous studies, gas with heavier methane carbon isotopes and high dryness coefficient can be generated at relatively low maturity (<2%) under the influence of instantaneous effects (Fig. 7(a) and (b)). However, assuming the accumulative gas generation process was more predominant, dry gas and heavy methane carbon isotopes can only be generated when the maturity of source rock reaches a much higher level than measured and modeled maturity range of the in-situ source rock in the study area (Fig. 7(a) and b) (Berner and Faber, 1996; Cramer et al., 2001; Guo et al., 2004; Geng et al., 2006; Li et al., 2008; Tian et al., 2023). Meanwhile, the organic carbon isotope of the source rock can also affect the generated natural gas carbon isotopes (Fig. 7(a)), and the average organic carbon isotopes of the Yuertusi Formation in the LT1 well is −30.25‰ (Zhu et al., 2021), which was used as reference value for gas generation modeling. The methane isotopes of actual samples are relatively similar to the instantaneous gas trends of fully open system Berner and Faber (1996), and the ethane isotopes of actual samples are relatively similar to the instantaneous gas trends of semi-open system (Chen et al., 2022), but neither is consistent with the trend for the accumulative gas (Fig. 7(a)). Therefore, the gas must be consistent with the instantaneous gas model, firstly. In the meantime, the actual geological conditions are unlikely to be fully open, it more likely to be an instantaneous gas generation in a semi-open system. Due to the complex hydrocarbon generating history of the source rocks and the variable open and closed conditions may be one of the reasons why the methane and ethane isotopes of the actual samples are consistent with the fully open and semi-open instantaneous gas trends, respectively, i.e., they are manifested as small differences in the methane and ethane carbon isotope values. Furthermore, section 5.1 has confirmed the natural gas exist leakage leads to the residual methane carbon isotopes becoming heavier, even partially heavier than the ethane carbon isotopes. It also leads to the range become smaller between methane and ethane carbon isotopes in the actual samples. Meanwhile the dryness coefficients are consistent with the instantaneous gas model (Fig. 7(b)). Therefore, it was shown that the presence of special natural gas properties in the Lunnan area, and the seemingly contradictory low maturity of the in-situ source rock can be best explained by the instantaneous gas generation effect and natural gas leakage.

5.4. The geological explanation for instantaneous gas generation

The generation of instantaneous effects may be related to fault activity, which determined the accessibility of vertical conduits for gas migration. During the key gas generation period, high-efficient fault activity provides favorable conduit pathways for the rapid migration of hydrocarbons from the source rocks to shallow reservoirs, resulting in instantaneous gas generation in the source rock.

The previous researchers have identified large-scale vertical penetrating fault activities in the Tabei uplift during the Late Caledonian, Late Hercynian, and Himalayan orogeny through U–Pb dating and 3D seismic techniques, even some of the faults penetrated from the Cambrian to the shallow strata, and these faults provided conduits for natural gas migration (Deng et al., 2019; Yang et al., 2020; Wu et al., 2021; Chen et al., 2022a; Cong et al., 2022; Jia et al., 2022). The hydrocarbon-generation simulation result shows that the late Hercynian orogeny and Himalayan orogeny are the two main periods of natural gas generation (Fig. 5). The thermal pulse

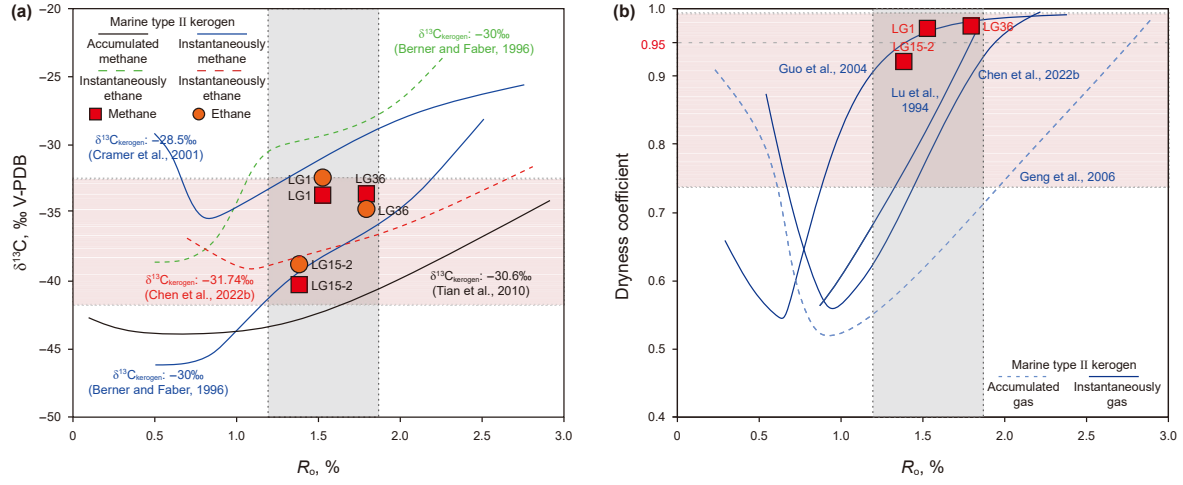

Fig. 7. Plot showing **(a)** source rock maturity (R_o%) vs. $\delta^{13}C$ and **(b)** source rock maturity (R_o%) vs. dryness coefficient for accumulated vs. instantaneous gas (after Lu et al., 1994; Berner and Faber, 1996; Cramer et al., 2001; Guo et al., 2004; Geng et al., 2006; Tian et al., 2010; Chen et al., 2020b).

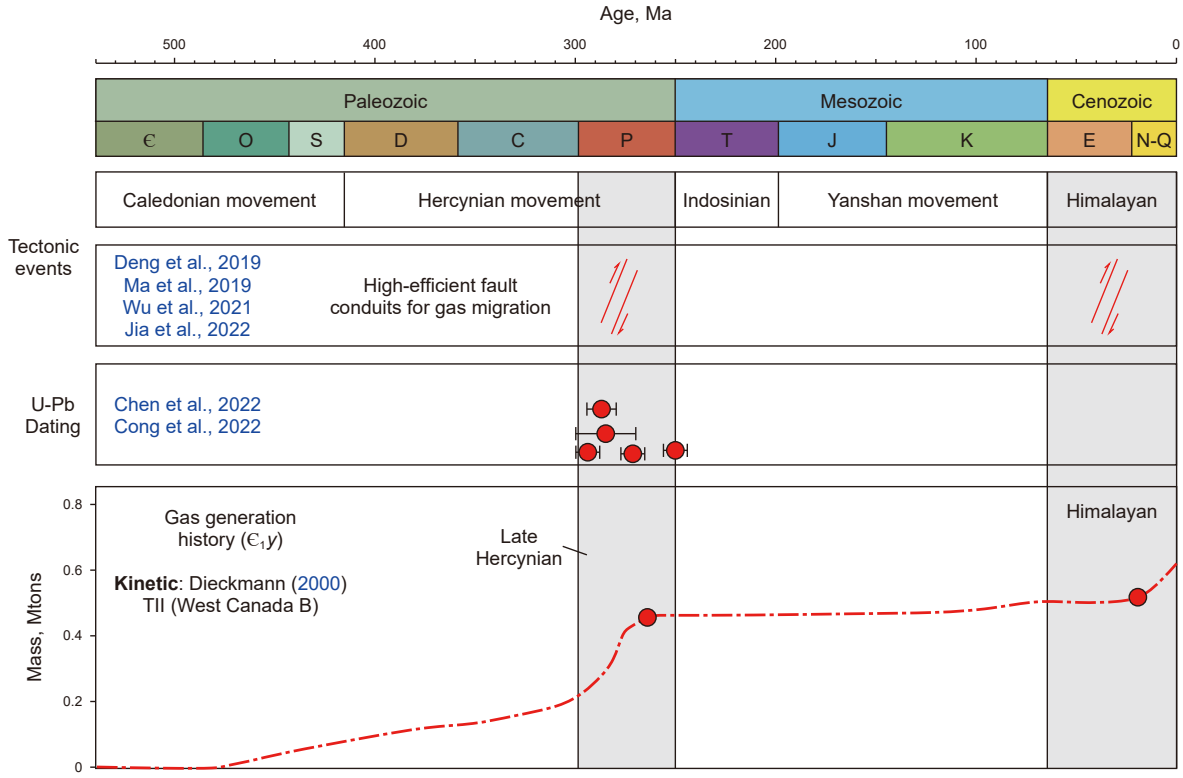

Fig. 8. Compilation of major tectonic events, U–Pb dating and natural gas generation history in the Tabei uplift since 540 Ma. Fault activity events and U–Pb dating are from Deng et al. (2019), Ma et al. (2019), Chen et al. (2022b), Wu et al. (2021), Cong et al. (2022), and Jia et al. (2022).

induced by the large igneous province during the Permian caused the maturity of the Yuertusi Formation source rocks in wells LG15-2, LG1, and LG36 to increase from 0.85%, 0.93%, and 1.02%–1.05%, 1.12%, and 1.20%, respectively, resulting in a significant generation of natural gas. However, as the strata suffered erosion in the Early Hercynian and Late Hercynian orogeny, causing the absence of Silurian, Devonian and Permian strata, the burial depth did not change much during the Late Hercynian to the Himalayan orogeny, the maturity of the in-situ source rock remained, without generating too much gas, and the Lunnan area also do not show obvious gypsum layer (Fig. 8). Therefore, the previously generated natural gas in the source rock and reservoirs have leaked due to active fault activity and poor sealing quality of cap rock. Till the Himalayan orogeny, rapid subsidence occurred, and the maturity of the in-situ source rock increased rapidly, propelling the generation of a significant amount of natural gas, which marked the main natural gas generation phase in the Lunnan area (Fig. 8). The high-efficient fault activity and favorable capping conditions in the Himalayan orogeny enabled the rapid migration of the generated natural gas into the reservoir and subsequent well preservation. As a result of the combined influence of fault activity, subsidence process, and natural gas generation process, all the current trapped natural gas in the Ordovician reservoirs of the Lunnan area should have been generated during the Himalayan orogeny. Long period pause in gas generation between the two hydrocarbon generation phases is the main reason for the formation of instantaneous effects.

6. Conclusions

1) The natural gas of the Lunnan area is mainly primary cracking gas with marine type II kerogen being the source. In the western area, the natural gas is dominated by wet gas, with relatively light methane carbon isotopes and low in-situ source rock maturity. In the eastern area, the natural gas is dominated by dry gas, with relatively heavy methane carbon isotopes and high in-situ source rock maturity.
2) The source rock maturity in the eastern and central areas corresponds to the stage of thermal cracking to generate condensate gas, but the natural gas properties in this area are inconsistent with the source rock maturity and exhibit instantaneous gas characteristics. The genesis of dry gas with relative heavy methane carbon isotopes at a low maturity level in the eastern and central areas are due to the instantaneous effects and natural gas leakage.
3) After the hydrocarbon generation phase during the late Hercynian orogeny, the burial depth did not change much over a long period of time until the Himalayan orogeny, and the lack of the gypsum layer, resulting in the leak of the early-generated wet gas. The natural gas present in the Ordovician reservoirs originated exclusively during the Himalayan orogeny. The significant interruption in gas generation between the two hydrocarbon production phases stands out as the primary reason for the formation of instantaneous effects.

CRediT authorship contribution statement

Xin Liu: Writing – review & editing, Writing – original draft, Investigation, Formal analysis, Data curation, Conceptualization. **Jin-Qiang Tian:** Writing – review & editing, Supervision, Investigation, Funding acquisition, Conceptualization. **Fang Hao:** Supervision, Funding acquisition. **Ze Zhang:** Investigation, Data curation. **Xian-Zhang Yang:** Resources. **Yong-Quan Chen:** Resources, Data curation. **Ke Zhang:** Resources, Data curation. **Xiao-Xue Wang:**

Resources, Data curation. **Fu-Yun Cong:** Writing – review & editing, Supervision, Investigation, Conceptualization.

Declaration of competing interest

The authors declare that they have no known competing financial interests or personal relationships that could have appeared to influence the work reported in this paper.

Acknowledgments

We thank three anonymous reviewers for their critical and constructive comments that improved the manuscript. We also thank the PetroChina Tarim Oilfield Company for their supports to this study. This research was financially funded by National Natural Science Foundation of China (Grant Nos. 41821002; 42172160); PetroChina (Grant No. ZD 2019-183-002); National Natural Science Foundation of China (Grant No. 42202142).

Appendix A. Supplementary data

Supplementary data to this article can be found online at https://doi.org/10.1016/j.petsci.2024.08.002.

References

Behar, F., Vandenbroucke, M., Tang, Y., et al., 1997. Thermal cracking of kerogen in open and closed systems: determination of kinetic parameters and stoichiometric coefficients for oil and gas generation. Org. Geochem. 26 (5–6), 321–339. https://doi.org/10.1016/S0146-6380(97)00014-4.

Behar, F., Vandenbroucke, M., Teermann, S.C., et al., 1995. Experimental simulation of gas generation from coals and a marine kerogen. Chem. Geol. 126 (3–4), 247–260. https://doi.org/10.1016/0009-2541(95)00121-2.

Berner, U., Faber, E., 1996. Empirical carbon isotope/maturity relationships for gases from algal kerogens and terrigenous organic matter, based on dry, open-system pyrolysis. Org. Geochem. 24 (10), 947–955. https://doi.org/10.1016/S0146-6380(96)00090-3.

Cao, J., Zhang, Y.J., Hu, W., et al., 2005. The Permian hybrid petroleum system in the northwest margin of the Junggar Basin, northwest China. Mar. Petrol. Geol. 22, 331–349. https://doi.org/10.1016/j.marpetgeo.2005.01.005.

Chen, J.Q., Ma, K.Y., Pang, X.Q., et al., 2020a. Secondary migration of hydrocarbons in Ordovician carbonate reservoirs in the Lunnan area, Tarim Basin. J. Petrol. Sci. Eng. 188, 106962. https://doi.org/10.1016/j.petrol.2020.106962.

Chen, J.Q., Pang, X.Q., Wu, S., et al., 2020b. Method for identifying effective carbonate source rocks: a case study from Middle -Upper Ordovician in Tarim Basin, China. Petrol. Sci. 17 (6), 1491–1511. https://doi.org/10.1007/s12182-020-00489-z.

Chen, J.X., Guo, X.W., Tao, Z., et al., 2022a. U-Pb dating of oil charge in superimposed basins: a case study from the Tarim Basin, NW China. GSA Bulletin 134 (11–12), 3176–3188. https://doi.org/10.1130/B36324.1.

Chen, L., Zheng, L.J., Huang, H.P., et al., 2022b. Carbon isotopic evolution of hydrocarbon gases generated from carbonate source rocks via different thermal simulation methods. Petroleum Geology & Experiment 44 (1), 121–128+138. https://doi.org/10.11781/sysydz202201121 (in Chinese).

Chung, H.M., Gormly, J.R., Squires, R.M., 1988. Origin of gaseous hydrocarbons in subsurface environments: theoretic considerations of carbon isotope distribution. Chem. Geol. 71, 97–104. https://doi.org/10.1016/0009-2541(88)90108-8.

Cong, F.Y., Tian, J.Q., Hao, F., et al., 2022. Calcite U-Pb ages constrain petroleum migration pathways in tectonic complex basins. Geology 50, 644–649. https://doi.org/10.1130/G49750.1.

Cong, F.Y., Tian, J.Q., Hao, F., et al., 2021. A Thermal pulse induced by a permian mantle plume in the Tarim Basin, Northwest China: constraints from clumped isotope thermometry and in situ calcite U-Pb dating. J. Geophys. Res. Solid Earth: JGR 126 (4), e2020JB020636. https://doi.org/10.1029/2020JB020636.

Cramer, B., Faber, E., Gerling, P., et al., 2001. Reaction kinetics of stable carbon isotopes in natural gas insights from dry, open system pyrolysis experiments. Energy Fuels 15 (3), 517–532. https://doi.org/10.1021/ef000086h.

Dai, J.X., Hu, G.Y., Ni, Y.Y., et al., 2009. Natural gas accumulation in eastern China. Energy Explor. Exploit. 27, 225–259. https://doi.org/10.1260/014459809789996147.

Dai, J.X., Ni, Y.Y., Zhang, W.Z., et al., 2016. Relationships between wetness and maturity of coal-derived gas in China. Petrol. Explor. Dev. 43 (5), 737–739. https://doi.org/10.1016/S1876-3804(16)30088-X.

Dai, J.X., Xia, X.Y., Li, Z.S., et al., 2012. Inter-laboratory calibration of natural gas round robins for δ^2H and $\delta^{13}C$ using off-line and on-line techniques. Chem. Geol. 310–311, 49–55. https://doi.org/10.1016/j.chemgeo.2012.03.008.

Deng, S., Li, H.L., Zhang, Z.P., et al., 2019. Structural characterization of intracratonic strike-slip faults in the central Tarim Basin. AAPG (Am. Assoc. Pet. Geol.) Bull. 103 (1), 109–137. https://doi.org/10.1306/06071817354.

Dieckmann, V., Horsfield, B., Schenk, H.J., 2000. Heating rate dependency of petroleum-forming reaction: implications for compositional kinetic predictions. Org. Geochem. 31, 1333–1348. https://doi.org/10.1016/S0146-6380(00)00105-4.

Fusetti, L., Behar, F., Bounaceur, R., et al., 2010. New insights into secondary gas generation from the thermal cracking of oil: methylated monoaromatics. A kinetic approach using 1,2,4-trimethylbenzene. Part I: a mechanistic kinetic model. Org. Geochem. 41, 146–167. https://doi.org/10.1016/j.orggeochem.2009.10.013.

Gao, B., Fan, M., Liu, W.H., et al., 2005. Carbon isotope features and genetic type of natural gas in Tahe oilfield. Oil Gas Geol. 26 (5), 618–622. https://doi.org/10.3321/j.issn:0253-9985.2005.05.010 (in Chinese).

Geng, X.H., Geng, A.S., Xiong, Y.Q., et al., 2006. Kinetic study of the hydrocarbon generation from marine carbonate source rocks characterization of products of gas and liquid hydrocarbon. Chin. Sci. Bull. 51 (23), 2885–2891. https://doi.org/10.1007/s11434-006-2197-7.

Guo, J.Y., Su, X.F., Wang, D.L., et al., 2004. Gas generation experimental research of shales, coal, bitumen and oil. Acta Sedimentol. Sin. S1, 110–117. https://doi.org/10.14027/j.cnki.cjxb.2004.s1.018 (in Chinese).

Harouna, M., Pigott, J.D., Philp, R.P., 2017. Burial history and thermal maturity evolution of the Termit Basin, Niger. J. Petrol. Geol. 40 (3), 277–297. https://doi.org/10.1111/jpg.12676.

Huang, H., Li, J., 2017. Molecular composition assessment of biodegradation influence at extreme levels — a case study from oilsand bitumen in the Junggar Basin, NW China. Org. Geochem. 103, 34–42. https://doi.org/10.1016/j.orggeochem.2016.10.005.

Jenden, P.D., David, R., Hilton, I.R., et al., 1993. Abiogenic hydrocarbons and mantle helium in oil and gas fields. In: Howell, D.G. (Ed.), The Future of Energy Gases. United States Government Printing Office, Washington, pp. 31–56.

Jia, C., Wei, G., 2002. Structural characteristics and petroliferous features of Tarim Basin. Chin. Sci. Bull. 47 (1), 1–11. https://doi.org/10.1007/BF0290281.

Jia, C.Z., Ma, D.B., Yuan, J.Y., et al., 2022. Structural characteristics, formation & evolution and genetic mechanisms of strizke-slip faults in the Tarim Basin. Nat. Gas. Ind. B 9 (1), 51–62. https://doi.org/10.1016/j.ngib.2021.08.017.

Jiang, L., Cai, C., Worden, R.H., et al., 2016. Multiphase dolomitization of deeply buried Cambrian petroleum reservoirs, Tarim Basin, north-west China. Sedimentology 63 (7), 2130–2157. https://doi.org/10.1111/sed.12300.

Jiang, Z.L., Jiang, S., Lan, X.D., et al., 2017. Neotectonic evolution of the Tarim Basin craton from neogene to quaternary. Int. Geol. Rev. 60 (10), 1–18. https://doi.org/10.1080/00206814.2017.1379365.

Jiang, Z.L., Huang, S.Y., Du, A.L., et al., 2015. The characteristics of the neotectonic movement and their effects on the formation of gas reservoirs in the marginal depressions of Tarim basin, NW China. J. Nat. Gas Sci. Eng. 22, 503–514. https://doi.org/10.1016/j.jngse.2014.12.028.

Li, M., Chen, Z., Yi, S., 2022. Origin and accumulation mechanisms of deep paleozoic oil and gas: a case study of the central Tarim basin, western China. J. Pet. Sci. Eng. 208, 109634. https://doi.org/10.1016/j.petrol.2021.109634.

Li, M.J., Wang, T.G., Chen, J.F., et al., 2010. Paleo-heat flow evolution of the Tabei uplift in Tarim Basin, northwest China. J. Asian Earth Sci. 37 (1), 52–66. https://doi.org/10.1016/j.jseaes.2009.07.007.

Li, X.Q., Xiao, X.M., Tang, Y.C., et al., 2008. The modeling of carbon isotope kinetics and its application to the evaluation of natural gas. Front. Earth Sci. China 2 (1), 96–104. https://doi.org/10.1007/s11707-008-0011-3.

Li, X.Q., Xiao, X.M., Tang, Y.C., et al., 2004. The generation and accumulation of natural gas from Yinan 2 gas pool in Kuqa Depression. Chin. Sci. Bull. 49, 107–114. https://doi.org/10.1007/BF02890462.

Li, X.L., Liu, S.W., Feng, C.G., 2019. Thermal properties of sedimentary rocks in the Tarim Basin, northwestern China. AAPG (Am. Assoc. Pet. Geol.) Bull. 103 (7), 1605–1624. https://doi.org/10.1306/11211817179.

Liao, Y.H., Zheng, Y.J., Pan, Y.H., et al., 2015. A method to quantify C1–C5 hydrocarbon gases by kerogen primary cracking using pyrolysis gas chromatography. Org. Geochem. 79, 49–55. https://doi.org/10.1016/j.orggeochem.2014.12.009.

Liu, Q.Y., Jin, Z.J., Li, H.L., et al., 2017. Geochemistry characteristics and genetic types of natural gas in central part of the Tarim Basin, NW China. Mar. Petrol. Geol. 89, 91–105. https://doi.org/10.1016/j.marpetgeo.2017.05.002.

Lorant, F., Prinzhofer, A., Behar, F., et al., 1998. Carbon isotopic and molecular constraints on the formation and the expulsion of thermogenic hydrocarbon gases. Chem. Geol. 147 (3–4), 249–264. https://doi.org/10.1016/S0009-2541(98)00017-5.

Lu, S.F., Zhao, X.G., Huang, D.F., et al., 1994. Modelling experiments on the generation and migration of coal-derived hydrocarbons: 1.the characteristics of gaseous and liquid hydrocarbon products and their evolutions. Exp. Pet. Geol. 16 (3), 290–302. https://doi.org/10.11781/sysydz199403290 (in Chinese).

Ma, D.B., Wu, G.H., Zhu, Y.F., et al., 2019. Segmentation characteristics of deep strike slip faults in the Tarim Basin and its control on hydrocarbon enrichment: taking the Ordovician strike slip fault in the Halahatang oilfield in the Tabei area as an example. Earth Sci. Front. 26 (1), 225–237. https://doi.org/10.13745/j.esf.sf.2019.1.10 (in Chinese).

Peng, P.A., Jia, C.Z., 2021. Evolution of deep source rock and resource potential of primary light oil and condensate. Acta Pet. Sin. 42 (12), 1543–1555. https://doi.org/10.7623/syxb202112001 (in Chinese).

Prinzhofer, A.A., Huc, A.Y., 1995. Genetic and post-genetic molecular and isotopic fractionations in natural gases. Chem. Geol. 126, 281–290. https://doi.org/

10.1016/0009-2541(95)00123-9.
Rooney, M.A., Claypool, G.E., Chung, H.M., 1995. Modeling thermogenic gas generation using carbon isotope ratios of natural gas hydrocarbons. Chem. Geol. 126 (3–4), 219–232. https://doi.org/10.1016/0009-2541(95)00119-0.
Schenk, H.J., Horsfield, B., 1993. Kinetics of petroleum generation by programmed-temperature closed-versus open-system pyrolysis. Geochem. Cosmochim. Acta 57 (3), 623–630. https://doi.org/10.1016/0016-7037(93)90373-5.
Schoell, M., 1980. The hydrogen and carbon isotopic composition of methane from natural gases of various origins. Geochem. Cosmochim. Acta 44, 649–661. https://doi.org/10.1016/0016-7037(80)90155-6.
Schoell, M., 1988. Multiple origins of methane in the earth. Chem. Geol. 71, 1–10. https://doi.org/10.1016/0009-2541(88)90101-5.
Stahl, J.W., 1973. Carbon isotope ratios of German natural gases in comparison with isotopic data of gaseous hydrocarbons from other parts of the world. In: Tissot, B., Bienner, F. (Eds.), Advances in Organic Geochemistry, pp. 453–462.
Stahl, W.J., Carey, J.B.D., 1975. Source-rock identification by isotope analyses of natural gases from fields in the Val Verde and the Delaware Basin, West Texas. Chem. Geol. 16, 257–267. https://doi.org/10.1016/0009-2541(75)90065-0.
Tang, Y., Perry, J.K., Jenden, P.D., et al., 2000. Mathematical modeling of stable carbon isotope ratios in natural gases. Geochem. Cosmochim. Acta 64 (15), 2673–2687. https://doi.org/10.1016/S0016-7037(00)00377-X.
Tian, H., Wu, Z.J., Gai, H.F., et al., 2023. Experimental study on late gas generation characteristics of the Middle Devonian sapropelic source rocks of in Northwestern Sichuan Basin. Oil Gas Geol. 44 (1), 46–54. https://doi.org/10.11743/ogg20230104 (in Chinese).
Tian, H., Xiao, X.M., Wilkins, W.T.R., et al., 2010. Genetic origins of marine gases in the Tazhong area of the Tarim basin, NW China: implications from the pyrolysis of marine kerogens and crude oil. Int. J. Coal Geol. 82 (1–2), 17–26. https://doi.org/10.1016/j.coal.2010.01.012.
Wang, D.W., Cai, C.F., Yan, L., et al., 2021. Geochemical evidence for secondary microbial gas in deep hot reservoirs of the Tarim Basin. Chem. Geol. 587, 120630. https://doi.org/10.1016/j.chemgeo.2021.120630.
Wang, X.M., Zhang, S.C., 2010. Petroleum characteristics and controlling factors in Lunnan low uplift, Tarim basin. J. Earth Sci. 21 (2), 236–246. https://doi.org/10.1007/s12583-010-0021-4.
Waples, D.W., 2000. The kinetics of in-reservoir oil destruction and gas formation: constraints from experimental and empirical data, and from thermodynamics. Org. Geochem. 31, 553–575. https://doi.org/10.1016/S0146-6380(00)00023-1.
Whiticar, M.J., 1999. Carbon and hydrogen isotope systematics of bacterial formation and oxidation of methane. Chem. Geol. 161 (1–3), 291–314. https://doi.org/10.1016/S0009-2541(99)00092-3.
Wu, M.L., Liu, Y.F., Peng, P., et al., 2021. Characteristics of strike-slip faults in Lunnan buried hill and its influence on hydrocarbon accumulation. Fault-Block Oil Gas Field 28 (4), 456–462. https://doi.org/10.6056/dkyqt202104005 (in Chinese).
Wu, N., Cai, Z.X., Yang, H.J., et al., 2013. Hydrocarbon charging of the Ordovician reservoirs in Tahe-Lunnan area. China. Sci. China Earth Sci. 56, 763–772. https://doi.org/10.1007/s11430-013-4598-1 (in Chinese).
Yang, F.L., Wang, T.G., Li, M.J., 2016. Oil filling history of the mesozoic oil reservoir in the Tabei uplift of Tarim Basin, NW China. J. Petrol. Sci. Eng. 142, 129–140. https://doi.org/10.1016/j.petrol.2016.02.005.
Yang, H.J., Wu, G.H., Han, J.F., et al., 2020. Structural analysis of strike-slip faults in the Tarim intracratonic basin. Chinese Journal of Geology 55 (1), 1–16. https://doi.org/10.12017/dzkx.2020.001 (in Chinese).
Yao, Z.W., He, G.Y., Li, C.F., et al., 2018. Sill geometry and emplacement controlled by a major disconformity in the Tarim Basin, China. Earth Planet Sci. Lett. 501, 37–45. https://doi.org/10.1016/j.epsl.2018.08.026.
Yu, C., Ni, Y.Y., Dai, J.X., et al., 2022. A comparison of the geochemical characteristics of ultra-deep natural gas in the kuqa foreland and marine craton areas in the Tarim Basin, China. Front. Earth Sci. 10, 884445. https://doi.org/10.3389/feart.2022.884445.
Yu, X., Yang, S.F., Chen, H.L., et al., 2011. Permian flood basalts from the Tarim Basin, Northwest China: SHRIMP zircon U-Pb dating and geochemical characteristics. Gondwana Res. 20 (2–3), 485–497. https://doi.org/10.1016/j.gr.2010.11.009.
Zhu, G.Y., Chen, F.R., Wang, M., et al., 2018. Discovery of the lower Cambrian high-quality source rocks and deep oil and gas exploration potential in the Tarim Basin, China. AAPG (Am. Assoc. Pet. Geol.) Bull. 102 (10), 2123–2151. https://doi.org/10.1306/03141817183.
Zhang, Z.Y., Wang, H., Zhu, G.Y., et al., 2022. Phase fractionation and oil mixing as contributors to complex petroleum phase in deep strata: a case study from LG7 block in the Tarim Basin, China. Mar. Petrol. Geol. 140, 105660. https://doi.org/10.1016/j.marpetgeo.2022.105660.
Zhao, G.J., Li, X.Q., Liu, M.C., et al., 2022. Accumulation characteristics and controlling factors of the Tugeerming gas reservoir in the eastern Kuqa Depression of the Tarim Basin, northwest China. J. Petrol. Sci. Eng. 217, 110881. https://doi.org/10.1016/j.petrol.2022.110881.
Zhou, F.Y., Zhang, S.C., 2000. Study on discharge history of well LN2 in Lunnan area, Tarim Basin: the evidence from fluid inclusion. Acta Petrol. Sin. 16 (4), 670–676. https://doi.org/10.3321/j.issn:1000-0569.2000.04.034 (in Chinese).
Zhu, G.Y., Li, J.F., Chi, L.X., et al., 2020. The influence of gas invasion on the composition of crude oil and the controlling factors for reservoir fluid phase. Energy & Fuels 34, 2710–2725. https://doi.org/10.1021/acs.energyfuels.9b03548.
Zhu, G.Y., Zhang, Z.Y., Zhou, X.X., et al., 2019. The complexity, secondary geochemical process, genetic mechanism and distribution prediction of deep marine oil and gas in the Tarim Basin, China. Earth Sci. Rev. 198, 102930. https://doi.org/10.1016/j.earscirev.2019.102930.
Zhu, G.Y., Zhang, B.T., Yang, H.J., et al., 2014. Origin of deep strata gas of tazhong in Tarim Basin, China. Org. Geochem. 74, 85–97. https://doi.org/10.1016/j.orggeochem.2014.03.003.
Zhu, G.Y., Milkov, A.V., Li, J.F., et al., 2021. Deepest oil in Asia: characteristics of petroleum system in the Tarim basin, China. J. Petrol. Sci. Eng. 199 (1), 108246. https://doi.org/10.1016/j.petrol.2020.108246.
Zhu, G.Y., Zhang, S.C., Liang, Y.B., 2009. The origin and distribution of hydrogen sulfide in the petroliferous basins, China. Acta Geol. Sin. 83, 1188–1201. https://doi.org/10.1111/j.1755-6724.2009.00139.x.